Design and Experimental Verification of Hip Exoskeleton With Balance Capacities for Walking Assistance

Ting Zhang, *Member, IEEE*, Minh Tran, and He Huang, *Senior Member, IEEE*

***Abstract*—Most current hip exoskeletons emphasize assistance for walking rather than stability. The goal of this paper is to develop a novel, high-power, self-balancing, and passively and software-controlled actively compliant hip exoskeleton that can assist with movement and maintain balance in both the sagittal and frontal planes. The developed hip exoskeleton includes powered hip abduction/adduction and hip flexion/extension joints. Each actuation unit employs a modular and compact series elastic actuator (SEA) with a high torque-to-weight ratio. It provides mechanical compliance at the interface between the exoskeleton and the wearer to ensure safety and a natural gait in the coupled wearer-exoskeleton system. A new balance controller based on the extrapolated center of mass concept is presented for maintaining walking stability. This controller reacts to perturbations in balance and produces a compliant guidance force through a combination of the passive elasticity of the SEA and active compliant control based on adaptive admittance control. The function of the hip exoskeleton is not to override human control, but rather to involve the wearer in movement control in order to avoid conflicts between wearer and exoskeleton. Our preliminary experiments on a healthy subject wearing the hip exoskeleton demonstrate the potential effectiveness of the proposed hip exoskeleton and controller for walking balance control.**

***Index Terms*—Balance control, exoskeleton, hip exoskeleton, series elastic actuator (SEA), walking assistance.**

I. Introduction

EXOSKELETONS are expected to expand the application of robotic technology to lower-limb rehabilitation. Various prototype lower-limb exoskeletons [1]–[3] have been developed; some of them have become commercially available, such as ReWalk [4], Ekso [5], HAL [6], and Indego [7]. These existing devices are primarily designed to restore mobility in paraplegic individuals. Commercial devices usually have powered joints (hip, knee, and/or ankle) in the sagittal plane. One limitation of the current exoskeletons is that they do not provide the function of maintaining the lateral stability of the coupled wearer-exoskeleton system. Usually, the wearer's balance is supported by crutches or a walker when the wearer is walking with an exoskeleton. The problem of how to design and control an exoskeleton that can effectively support the wearer-exoskeleton system's stability during upright locomotion remains an open question [3].

In the biomechanics of human locomotion, the control of foot placement in both the mediolateral and anteroposterior directions has long been recognized as an effective mechanism for maintaining bipedal gait stability [8]. During walking, beyond the forward step length regulated by hip flexion/extension (HFE), adaptation of the step width, which can be adjusted by hip abduction/adduction (HAA) motions, is also crucial for walking stability. A lateral weight shift and HAA motions have been shown to precede the initiation of a forward step [9]. Biomechanical studies have indicated that the step width and the mediolateral foot placement at the end of each step can be estimated based on the center of mass (CoM), which is assumed to be located at the pelvis [10]. The extrapolated center of mass (XCoM) is obtained by vertically projecting the CoM's position to the ground in the direction of its velocity [11]. More specifically, the XCoM combines information about the current kinematics data of the CoM to predict a future time at which the CoM will contact the support boundary. Because the XCoM has been validated in both static and dynamic situations, it can be used as a flexible spatial variable in the formulation of conditions for stability during walking [12]. In the presence of perturbations and other dynamic postural conditions, the XCoM is an important parameter in determining whether an additional step is required to maintain balance [13]. The XCoM concept has been successfully applied in analyzing human balance control [14].

Several solutions for addressing wearer-exoskeleton stability in locomotion have recently been proposed. Li *et al*. designed an additional balance stabilizer mechanism that can be attached to the wearer to enhance the stability of the wearer-exoskeleton system [15]. However, the additional stabilizer is large in size and weight, which may further limit the mobility of the wearer. Compliant actuation has been used in full-body exoskeletons to produce relatively stable and natural gaits, but the size and complexity of such exoskeletons significantly limits their

Manuscript received May 10, 2017; revised July 25, 2017 and October 9, 2017; accepted January 2, 2018. Date of publication January 5, 2018; date of current version February 14, 2018. Recommended by Technical Editor H. A. Varol. This work was supported in part by the National Science Foundation under Grant 1406750 and in part by North Carolina State University Faculty Scholar Program. *(Corresponding author: Ting Zhang.)*

The authors are with the Joint Department of Biomedical Engineering, North Carolina State University and the University of North Carolina at Chapel Hill, Raleigh, NC 27695 USA (e-mail: zhangt.hit@gmail.com; mqtran2@ncsu.edu; hhuang11@ncsu.edu).

Color versions of one or more of the figures in this paper are available online at http://ieeexplore.ieee.org.

Digital Object Identifier 10.1109/TMECH.2018.2790358

mobility [16], [17]. Since hip and ankle joints are critical for balance and upright stability in humans [18], several studies have attempted to advance hip and/or ankle design and control to address wearer-exoskeleton stability. Ugurlu *et al*. exploited variable ankle stiffness to improve a bipedal exoskeleton's balance control [19]. Unfortunately, the lower-limb exoskeleton used in these experiments was effectively a bipedal robot that did not include the human wearer in the loop. Hip torque in the frontal plane was used to counteract the momentum arising from gait perturbations such as trips and slips. Wang *et al*. developed an exoskeleton with active HAA to adapt step width and counteract gait disturbances in the frontal plane based on the XCoM concept [20], [21]. Their work focused on spinal cord injury paraplegics, and thus the controller was formulated to track a predefined gait trajectory. This method is appropriate and effective for paraplegics but will present problems to wearers who still have voluntary motor control because the forced motion applied to the human joints may conflict with users' effort. Furthermore, only perturbations from the stance side during single support were considered, whereas disturbances could also come from the swing side during locomotion.

An important feature of exoskeleton systems, which distinguishes them from bipedal robots, is the participation of the wearer in the locomotion, balance control, and decision-making processes [19]. If the wearer has muscular weakness but still retains voluntary motor control of their lower limbs for balance recovery, inappropriately applied exoskeleton's assistive torque applied to the human joints may conflict with the natural way of walking, thus causing an increase in the effort needed for walking or even will causing fall. How much mechanical assistance is appropriate for balance recovery is still an open question for wearable robot control in general. Research has shown that wearers with voluntary motor control ability will inadvertently modulate their own muscle torques when the coupled wearer-exoskeleton system is losing balance under perturbation [22]. Moreover, muscle efforts required to maintain balance vary among users, and even in the same user under different circumstances. An ideal exoskeleton controller for balance assistance should therefore continuously adapt to the wearer's intentions and movements to (1) provide appropriate assistance upon disturbances or at the wearer's request and (2) present high levels of transparency under no-assistance conditions [23].

Inspired by human biomechanics, the objective of this study was to develop a novel hip exoskeleton that can actively control HFE and HAA to ensure the wearer's walking stability. Hip exoskeletons [24]–[31] have received increasing research attention in recent years, and some devices have become commercially available, such as the suitX Phoenix [25]. This is because the hip is important for powering upright locomotion and postural control, and compared with a powered ankle, hip exoskeletons add minimal inertia to the leg and, therefore, only slightly affect the lower-limb dynamics. To address the human-in-the-loop balance control challenges for a hip exoskeleton and achieve our study goal, we designed a controller that reacts to balance perturbations and produces a compliant guidance force through a combination of series elastic actuator (SEA) passive elasticity and active compliant control based on adaptive admittance control. SEAs are widely used in robotics and advantageous for ensuring safety because of their ability to efficiently achieve mechanical compliance between the actuators and the wearer-exoskeleton interface [32]. Many upper limb and lower-limb exoskeletons have used SEAs [24], [33]–[38]. In addition, our exoskeleton is designed not to override human control but rather to involve the wearer in movement control to avoid conflicting with the wearer.

The contributions of this paper are as follows.

1) Design a SEA-driven hip exoskeleton with powered HAA and HFE joints to maintain balance in both sagittal and frontal planes.
2) We integrated the XCoM concept with admittance control to assist with HAA to broaden step width and also to provide assistance in lateral weight shift to improve lateral stability.

The balance control scheme applied with human-in-the-loop is built upon the "assist-as-needed" (AAN) paradigm. The hip exoskeleton applies an AAN compliant guidance force on the HAA, based on the subjects' performance, to improve lateral stability and avoid conflicts between wearer and exoskeleton during use.

This paper is organized as follows. The design requirements for the hip exoskeleton are presented in Section II. The design and hardware description of the hip exoskeleton are presented in Section III. In Section IV, we describe the design of the hip exoskeleton control system. Section V presents an experimental evaluation and its results. A discussion and conclusion are given in Sections VI and VII, respectively.

II. Requirements

The work presented in this paper serves as a research prototype to further advance the state of the art in hip exoskeletons and controllers. This technology aims to promote stable walking in patients who have muscular weakness but retain voluntary lower-limb motor control. The final goal is to create a hip exoskeleton platform that can enable the development of exoskeletons with more flexible and adaptive behavior. We defined the following list of requirements for the new hip exoskeleton, based on the stated goal and our rehabilitation experience:

A. Kinematic and Dynamic Requirements

During human walking, step-width adaptation and weight shift are crucial for maintaining lateral stability [8]. However, individuals with muscular weakness may have difficulty performing these stability tasks. Thus, to support the wearer and maintain balance in both the sagittal and frontal planes, both the HAA joints and the HFE joints must be powered. The exoskeleton needs to support a walking speed of up to 0.8 m/s. The dimensions of the device should accommodate the hip width and other anthropometric features within the 5%–95% range of the adult population as detailed in [21].

The design parameters of the actuation unit (summarized in Table I) are critical for meeting the kinematic and dynamic requirements of the hip exoskeleton. For an 80-kg person, each actuator should provide a continuous torque of 40 N·m, a maximum torque of 80 N·m and a maximum joint velocity of 150 deg/s based on the hip angle and torque profiles from the

TABLE I
DESIGN REQUIREMENTS FOR HIP EXOSKELETON ACTUATION [21]

#	Item	Desired value	
		HFE	HAA
R1	Range of motion	+110/−18	19/–22
R2	Continuous torque	40 N·m	
R3	Peak velocity	150 deg/s	
R4	Output torque resolution	1 N·m	
R5	Joint mass	As light as possible	

Winter dataset [18]. The device is expected to generate up to 50% of the torque required during human ground-level walking at a natural cadence of 105 steps/min [19]. We adopted an exoskeleton mass limit of 12 kg that is similar to other commercial hip exoskeletons, such as the suitX Phoenix [25], that are designed to help people with mobility impairments to stand upright and walk.

B. Compliant Interaction Requirements

The exoskeleton should be able to produce controllable mediolateral forces on the legs during walking. Incorporating compliance is also important for the exoskeleton when considering dependability, intrinsic stability, inherent safety, energy management, and environmental adaptability [3].

Given its close interactions with its human wearer, the exoskeleton should be compatible with the user's range of joint motion, anthropometry, and kinematics to provide a good fit and a comfortable physical human–robot interface [7]. In addition, the exoskeleton's actuation and control should allow the wearer to perform his or her own movements without hindrance while still safely receiving assistance.

C. Balance Control Requirements

Besides the machine design, the balance controller is important for maintaining balance in both the sagittal and frontal planes and should consider the human–machine interaction. The exoskeleton controller should assist the wearer in achieving dynamic stability during walking. To maintain lateral balance, the controller must continuously monitor and adjust the HAA movement during the swing phase to correct the step width and weight shift. In the case of perturbations from either external sources or the wearer's own motions, the exoskeleton will assist with changing foot placement position to widen/narrow the step width to counter balance losses.

III. DESIGN DESCRIPTION

This section highlights several aspects of the hip exoskeleton design, namely, the mechanical structure, actuation units, sensor system, human–exoskeleton attachment, electrical hardware, and safety.

A. Mechanical Structure

The mechanical design of the hip exoskeleton is illustrated in Fig. 1. The articulation of the hip exoskeleton is achieved about four single-axis revolute joints: one for each HFE joint, mounted on the lateral arm, and one for each HAA joint. The HAA and HFE joints can work simultaneously to maintain balance in both the sagittal and frontal planes. The powered joints have a modular design, and additional modules can be attached or removed to change the joint behavior and adapt to a patient's progress and abilities. The hip exoskeleton, excluding the battery unit, has a total weight of 9.2 kg and, through an adjustable mechanism, conforms to wearers over a wide range of body sizes.

B. SEA-Actuation Units

Because of the size limit for exoskeleton actuators and the requirement for high torques while operating at higher speeds, most types of actuators used in robotics cannot be used. To accommodate the power and weight requirements, the actuation system for our prototype, including the power electronics and actuators, was custom made, as shown Fig. 1. For wearable devices, especially lower-limb exoskeletons, the power-to-weight, and torque-to-weight ratios of the actuators must be maximized to minimize the device weight. Therefore, special efforts were devoted to the actuation system design.

The SEA is driven by a flat brushless motor and a harmonic drive gear. The motor is a Maxon rotating flat brushless dc motor (EC 90 flat, Maxon Motor, Sachseln, Switzerland) equipped with an incremental encoder (4095ppr, MILE, Maxon Motor, Sachseln, Switzerland), with a continuous torque rating of 0.44 N·m. The transmission ratio of the harmonic gearbox (csd-25-100-2A-GR-BB, Harmonic Drive, Limburg, Germany) is 100:1, resulting in an output torque of approximately 40 N·m, an output velocity of 150 deg/s, and a peak torque of approximately 80 N·m for durations on the order of a few seconds (thermally limited). The series spring is a torsional spring that was specially developed to achieve the target stiffness (2.15 N·m/deg) with minimal weight. This spring has a double-spiral disc shape and is made of a single piece of high-grade titanium. Each SEA weighs approximately 1.5 kg, of which the motor contributes 0.6 kg.

C. Sensor System

To accomplish the compliant control scheme, the series elastic actuated joints are equipped with numerous sensors. Each joint is equipped with both kinematic (angular position, velocity and acceleration) and kinetic (interaction force between limb and exoskeleton) sensors.

The physical sensing of the hip exoskeleton is performed using the following.

1) Absolute position magnetic encoders (MBA8, AksIM^{TM} rotary absolute encoder module, RLS, Komenda, Slovenia) at each joint output shaft measuring the joint angle.
2) A torque sensor at each powered joint measuring the interaction torque between the body of the human user and the exoskeleton joint.
3) Three Inertia Measurement Units (IMUs) (VN-100S, Vectornav Embedded Navigation Solutions, Dallas, TX, USA) place at the back of the exoskeleton (near the CoM

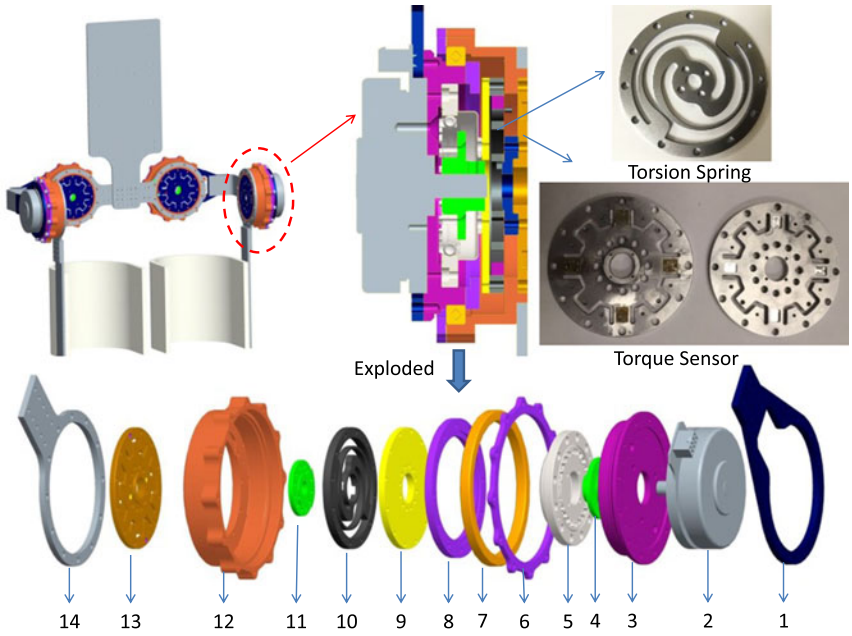

Fig. 1. Mechanical design. 1-link, 2-motor, 3-flange, 4-coupling, 5-Harmonic Drive, 6-bearing outer bezel, 7-bearing, 8-bearing inner bezel, 9-connector with spring, 10-torsion spring, 11-link between torsion spring and torque sensor, 12-shell, 13-torque sensor, 14-link.

position of the human body) and left and right ankles to estimate the XCoM.

4) Resistive foot-pressure sensor arrays (FSR 402, Interlink Electronics, Camarillo, CA, USA) embedded in the left and right shoe insoles that act as switches to detect foot-ground contact and foot-off events, which are used to distinguish the stance and swing phase.

The structure of the torque sensor and finite element analysis (FEA) results are shown in Figs. 1 and 2, respectively. The four strained beams are cross shaped and the rectangular groove is machined on each strained beam as an elastomer to sense strain. The FEA analysis was set up with the inner ring fixed, and an external torque was applied on the outer ring (torque directions are shown with white arrows). The results showed that the maximum stress and strain due to the torque both occurred in the middle region of the strain beam's rectangular groove. When the maximum torque was 67.8 N·m, the maximum stress was 174.304 MPa and the maximum strain was 2.274×10^{-3}. The maximum calculated stress of the torque sensor is much less than the shear strength of 7075T6 aluminum alloy. Thus, the designed torque sensor fully meets the strength requirements for our hip exoskeleton application.

Two strain gauges (for example S1 and S2) are fixed to the back of the rectangular groove of each strained beam. They form on the two 180° strain girders a full Wheatstone bridge, so a total of two full Wheatstone bridge circuits are present in the sensor. The two full bridges will improve the sensor's reliability and reduce measurement errors due to thermal effects, as previously reported [39]. In addition, the orthogonal arrangement of the cross shape allows easy algebraic averaging of the two bridges' output, which can offset torque ripples caused by the harmonic reducer. Strain gages (N2A-06-T029H-350, Shear/Torque Rosettes, MICRO-MEASUREMENTS,) are used in the torque sensor. The strain gauge's resistance is 350 Ω, and the strain coefficient is 2.06%, which results in high sensitivity, small drift, and good thermal stability. An instrumentation amplifier (INA337, Texas Instruments, Dallas, TX, USA) is used in each Wheatstone bridge. The bridge is excited with 5-V dc power supply, and a custom-made electronic circuit balances the bridge for null-point measurements and also amplifies the output by a factor of 100. The amplifier circuit contains a 312 Hz low-pass filter circuit to reduce the noise before analog-to-digital conversion. The linearity, hysteresis, and sensitivity of the torque sensor are 2.19%, 3.06%, and 0.41, respectively. Sensor noise was experimentally determined to be ±0.22 N·m, about 0.16% of the torque capacity.

D. Human–Exoskeleton Attachment

The exoskeleton is easy to don and doff and attaches to the wearer at three main locations: leg, pelvis, and torso. Thigh braces are used to loosely constrain the upper leg and support sit-to-stand. The exoskeleton backpack is secured to the user's body with pelvis and shoulder straps. Three cuffs per leg, two at the calf and one at the thigh, attach the exoskeleton to the leg. To accommodate different users, the design includes several adjustable mechanisms including telescopic structures in the thigh and shank and a sliding rail system at the pelvis.

E. Electrical Hardware

The electrical system of the hip exoskeleton is responsible for high-level control, low-level brushless motor control, sensor signal acquisition and processing, and communication. Fig. 3 shows the electrical hardware structure of the hip exoskeleton. Each joint is equipped with one 150-W commercial brushless motor driver (Copley Accelnet digital drive) to drive the motor and to provide feedback of the encoder and motor current data to the high-level control system. Each joint also uses a mini DSP chip to acquire data from the joint position and torque sensors. The high-level control system runs on a laptop. A CAN

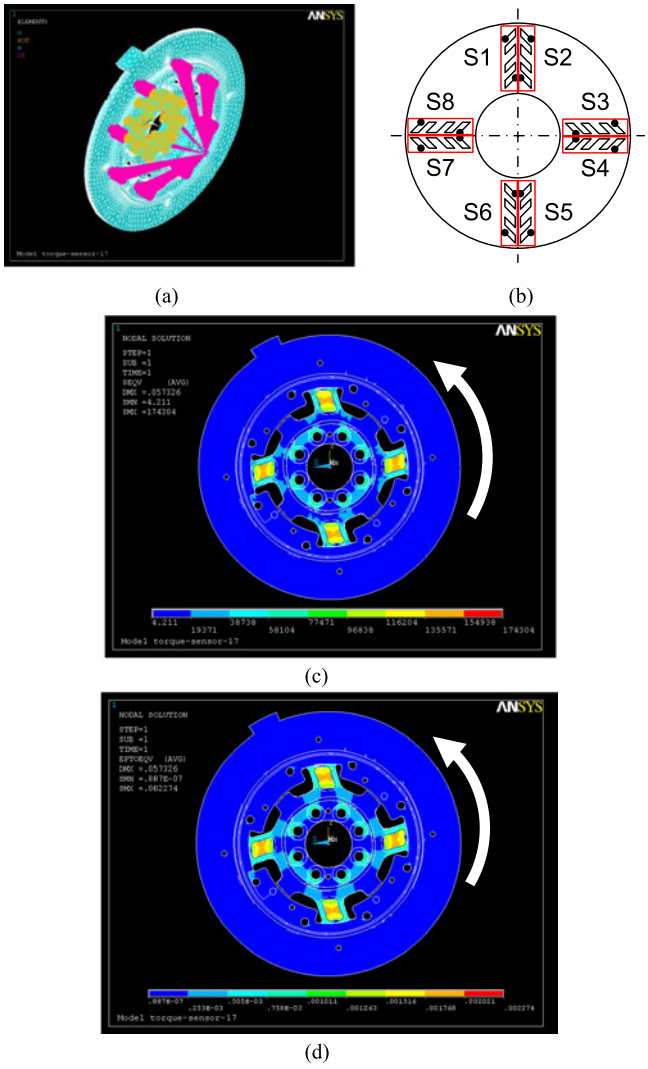

Fig. 2. FEA of torque sensor. (a) Mesh grid used in FEA. (b) Arrangement of strain gauges. (c) Stress distribution for a torsional moment of 60 N·m. (d) Deflection distribution for a torsional moment of 60 N·m.

bus connects all elements of the hip exoskeleton, including the high-level and low-level control systems. An acquisition board (USB-1208FS, Measurement Computing, Norton, MA, USA) connected to a PC is used to acquire the signals from the resistive foot-pressure sensor. The lower-level control loop is updated at 2 kHz, with an inner current loop that is updated at 10 kHz, and the control parameters are updated by the high-level controller at 100 Hz. All high-level control algorithms are implemented in *C#* in Microsoft Visual Studio for real-time control. The electrical system is powered by a 24-V benchtop dc power supply.

F. Safety

To ensure the safety of both the wearer and the device, various mechanical, electrical, and software-related safety protections must be considered in exoskeleton design [34]. The safety is ensured through software supervision as well as protection features within electronic and mechanical systems. The software supervision and electronics provide active protection, whereas the mechanical protection is passive.

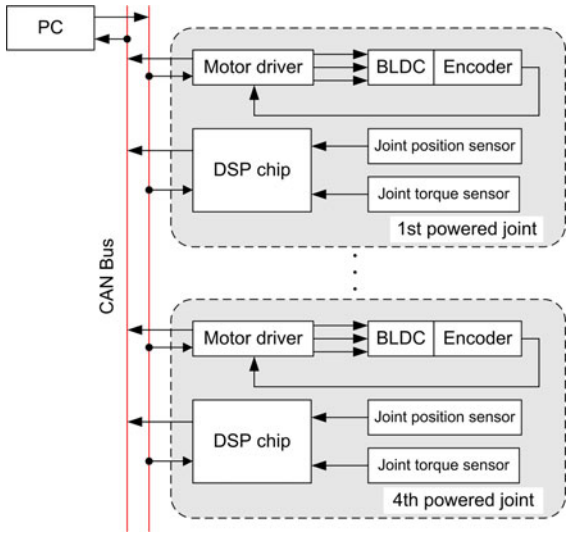

Fig. 3. Electrical hardware structure.

1) Active Protection: The control software continuously monitors each SEA module's velocity, motor current and temperature, torque and position sensor readings, and communication status. If any reading is out of the safe ranges and/or incorrect, the drivers will stop the motors and display a warning.
2) Passive Protection: The hip exoskeleton features mechanical end stops for all four powered joints to prevent the device from exceeding its specified ranges of motion. The SEAs are also backdrivable, and the exoskeleton has no sharp edges.

IV. Controller Description

The exoskeleton controller must perform two main tasks: assistive walking and maintaining walking stability. Accordingly, the hip exoskeleton's control strategy was subdivided into strategies for locomotion and balance control.

As implemented in the controller, a finite-state machine governs the walking behavior of the hip exoskeleton. During normal assistive walking, the hip exoskeleton is controlled by a high-level control scheme based on a conventional finite-state machine, and a low-level control scheme based on admittance control. If any loss of stability is detected, the exoskeleton will immediately add a new control input to prevent the wearer from losing stability.

The details of the assistive control in the sagittal plane (HFE) and the SEA trajectory-tracking controller have been reported in a previously submitted paper [40]. The assistive control scheme allows the wearer to select a step length and time that maintain his or her zero-moment point within a support polygon. The focus of the current paper is the design and implementation of a balance control scheme to improve lateral balance.

A. Finite-State Machine

Five gait-phase states are defined for assisted walking: left-leg early swing (flexion), left-leg late swing (extension), double support, right-leg early swing (flexion), and right-leg late swing

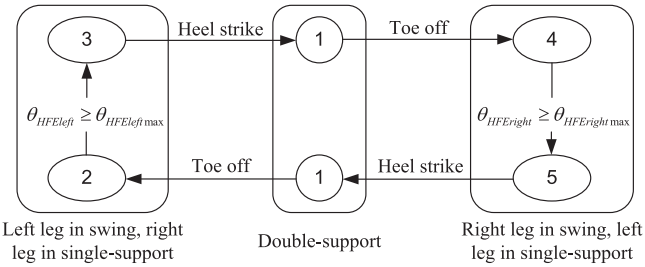

Fig. 4. Finite state machine switching conditions.

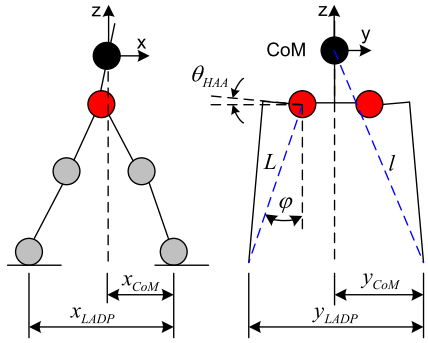

Fig. 5. Sketch of the estimation of the CoM position in the sagittal plane and in the frontal plane.

(extension). Each state consists of parameters describing the impedance of the four hip joints, including the joint stiffness (K), damping (D), and equilibrium angle (θ_0), as well as transition criteria. During operation, the states are concatenated to produce seamless locomotion behavior. An admittance-based controller was chosen to cooperatively render the joint impedance with the integrated series compliance within the SEA mechanism.

A finite-state machine, as shown in Fig. 4, uses the outputs from an inertial measurement unit (IMU) and resistive foot-pressure sensor to estimate the switching conditions between the finite states of the state machine. The gait phase switches from single-support to double-support states via detection of heel strike of the respective swing leg, which can be measured by resistive foot-pressure sensors. The gait phases are: 1-double support, 2-left-leg early swing (flexion), 3-left-leg late swing (extension), 4-right-leg early swing (flexion), and 5-right-leg late swing (extension). Switching between 2 and 3, or 4 and 5, is done by comparing current HFE angles with maximum hip flexion angle for each leg. An IMU was attached on the front of each thigh to measure the maximum hip flexion angle in real time. The stride time is measured by the hip exoskeleton controller's timer as the time between two consecutive heel strike events on the same foot. The expected maximum hip flexion angle is estimated from the average of the previous two strides. The maximum hip flexion angles and the maximum hip extension angles at the first two strides are measured by joint angle sensors during walking at zero-torque control mode. Maximum hip flexion angles are updated in real time within the admittance controller [39], which is based on the interaction torque between the hip exoskeleton and wearer.

B. Balance Control

We first define a ratio to detect the disturbance [20]

$$r_{\text{lateral}} = \frac{y_{\text{CoM}}}{y_{\text{LADP}}} \tag{1}$$

where r_{lateral} is the weight shift ratio in the frontal plane; y_{CoM} and y_{LADP} are the CoM position and step width, respectively, in the frontal plane, as shown in Fig. 5.

In the concept of XCoM, the single stance phase of a bipedal gait is modeled as an inverted pendulum [12]. According to the XCoM concept [12], the XCoM position in the lateral plane is defined as

$$\text{XCoM}_y = \text{CoMy} + \frac{v_{\text{CoMy}}}{\omega_0} \tag{2}$$

where CoMy and v_{CoMy} are the lateral CoM position and velocity, respectively, and ω_0 is the eigenfrequency of the pendulum $\omega_0 = \sqrt{g/l}$, where l is the length of the pendulum and g is the acceleration due to gravity. L is the distance between the swing HAA and foot. φ is the angle between L and gravity.

The deviation of the XCoM position is

$$\begin{aligned}\Delta\text{XCoM}_y &= \Delta\text{CoMy} + \frac{\Delta v_{\text{CoMy}}}{\omega_0} \\ &= \text{CoMy} - y^{bs}_{\text{CoM}} + \frac{v_{\text{CoMz}} - v^{bs}_{\text{CoMz}}}{\omega_0}\end{aligned} \tag{3}$$

where y^{bs}_{CoM} and v^{bs}_{CoMy} are the averaged value of the CoMy and v_{CoMy} at certain period in the swing phase during normal walking gait without any perturbation, respectively. Δv_{CoMy} is the acceleration of CoMy.

To return the XCoM to its nominal value to counteract the perturbation, the change HAA angle should be equal to the deviation of the XCoM position [21]

$$\Delta\text{XCoM}_y = L\left(\sin\left(\Delta\theta_d^{\text{HAA}} + \varphi\right) - \sin\varphi\right) \tag{4}$$

So, when r_{lateral} exceeds predefined thresholds, the HAA adjustment angle is

$$\Delta\theta_d^{\text{HAA}} = \arcsin\left(\frac{\Delta\text{XCoM}_y}{L} + \sin\varphi\right) - \varphi. \tag{5}$$

The step width is adjusted only during the swing phase (single support), and two adjustment strategies are used, depending on the tilt direction during the swing phase. For the left-leg swing phase (right-leg support), when r_{lateral} is below the lower threshold (the CoM is tilted to the right side of the sagittal plane), the powered HAA adjustment angle is

$$\begin{cases}\theta_{k+1}^{\text{LeftHAA}} &= \theta_k^{\text{LeftHAA}} + \Delta\theta_d^{\text{HAA}} \\ \theta_{k+1}^{\text{RightHAA}} &= -\theta_{k+1}^{\text{LeftHAA}}\end{cases}. \tag{6}$$

This adjustment will result in greater hip abduction at heel strike and a larger step width to recover balance. By contrast, when r_{lateral} exceeds the upper threshold (the CoM is tilted to

the left side of the sagittal plane), the powered HAA adjustment angle is

$$\begin{cases} \theta_{k+1}^{\mathrm{LeftHAA}} &= \theta_{k}^{\mathrm{LeftHAA}} + \Delta\theta_{d}^{\mathrm{HAA}} \\ \theta_{k+1}^{\mathrm{RightHAA}} &= a\Delta\theta_{k+1}^{\mathrm{LeftHAA}} \end{cases} \tag{7}$$

where a is a proportionality factor. This HAA adjustment will shift the CoM to the left to recover balance. The behavior during the right-leg swing phase is similar. A similar control law is applied to right-leg swing.

C. Adaptive Admittance Control

The low-level control layer implements an adaptive admittance controller to achieve assistance as needed. The admittance controller consists of an admittance model followed by an SEA trajectory-tracking controller [40].

The balance controller output is target adjustment angles of both HAA angles. The adaptive admittance controller considers the interaction torque between the wearer and the exoskeleton to produce an adaptive assistance torque to achieve balance controller outputs. The adjusted reference trajectory θ_{adj} is given by (7), where s is the Laplace operator

$$\begin{cases} \theta_{adj} &= \theta_0 + \theta_{\mathrm{int}} \\ \theta_{\mathrm{int}} &= -A(s)\tau \\ \frac{A(s)}{s} &= \frac{1}{K+sD} \end{cases} \tag{8}$$

where θ_{int} is the angle related to the interaction torque τ between the exoskeleton and the wearer's joint. This angle is estimated using the virtual impedance parameters D and K of the exoskeleton, and it increases or decreases proportionally to the interaction torque between the wearer and the exoskeleton. An increase in the interaction torque indicates a greater difference between the trajectory of the wearer's limb and the trajectory of the exoskeleton.

The concept of assistance as needed is implemented by varying the joint stiffness. The variation in stiffness can be determined based on the performance of the wearer and the level of assistance to be exerted by the hip exoskeleton

$$\begin{cases} K_{T+1} &= K_T + \Delta K \\ \Delta K &= \frac{\theta_0 - \theta}{\varepsilon\tau} \end{cases} \tag{9}$$

where ε is a confidence factor in the interval [0, 1], which is used to determine the stiffness to be applied at sample time $T+1$. A low confidence factor means that partial or complete balance assistance should be provided, whereas a higher confidence factor indicates that the subject is capable of balance control with little or no assistance.

V. Experiments and Results

In this section, we describe the results of experiments conducted to characterize the performance of the proposed hip exoskeleton and controller. First, we demonstrate the exoskeleton's performance characteristics. Second, we present the validation results for the controller.

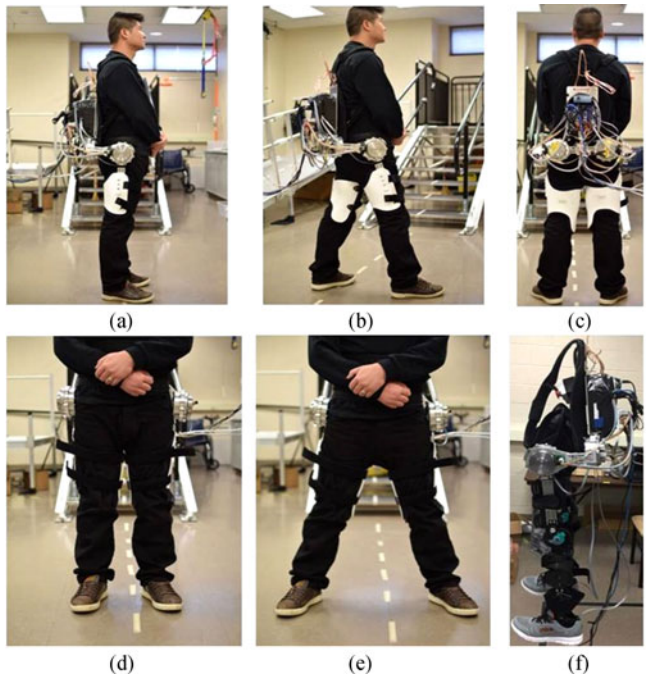

Fig. 6. Developed 4-DOF hip exoskeleton. (a) Side view. (b) Side view with hip flexion. (c) Back view. (d) Front view. (e) Front view with hip abduction. (f) Hip exoskeleton with standard knee-ankle-foot orthosis.

A. Exoskeleton System Performance

A picture of the assembled hip exoskeleton is shown in Fig. 6. The torque and speed performance characteristics of the powered joints of the hip exoskeleton were experimentally quantified. The hip exoskeleton was connected to a standard knee-ankle-foot orthosis to support its weight [see Fig. 6(f)].

Because of the high transmission ratio of the SEA, the maximum angular velocity of each joint is limited by the motor driver of the motor, which operates at 24 V. The maximum joint angular velocity of the powered joints, as measured using motor Hall sensors, is approximately 150 deg/s. The maximum output (i.e., the continuous torque of the powered joints as measured using joint torque sensors) is approximately 40 N·m.

The torque–angle relationship of the SEA with no control under loading and unloading, i.e., with the motor turned off, is shown in Fig. 7. The figure demonstrates that the joint is backdrivable even with no power. The slope of the red line represents the desired design stiffness, and the actual results are shown in blue. The relationship was nearly linear (nonlinearity is 2.12%), and the hysteresis was small (4.81%). The results demonstrate that the SEA satisfies the design objective, with a stiffness of 2.156 N·m/deg.

Three experimental trials were conducted to validate the admittance controller. During these trials, a dynamic external force (pulling and pushing at a frequency of less than 2 Hz) was manually exerted on the pivoting link. The stiffness was set to values of 0 N·m/deg (zero-torque control mode), 0.2 Nm/deg, and 0.5 N·m/deg. When $K = 0$, the interaction torque was very close to zero. The absolute torque value was smaller than 1.3 N·m with the stiffness set to 0. At a low frequency, the interaction

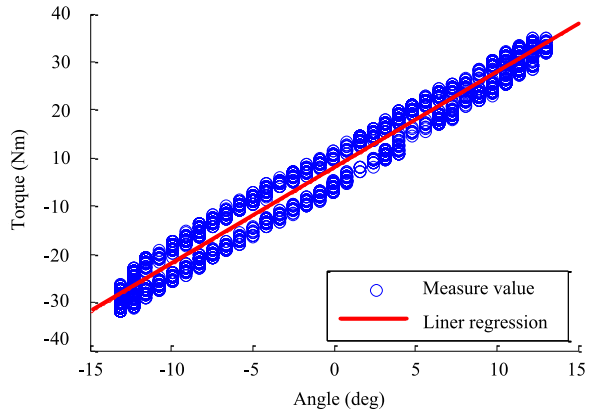

Fig. 7. Torque-angle relationship of the SEA without active control under loading and unloading.

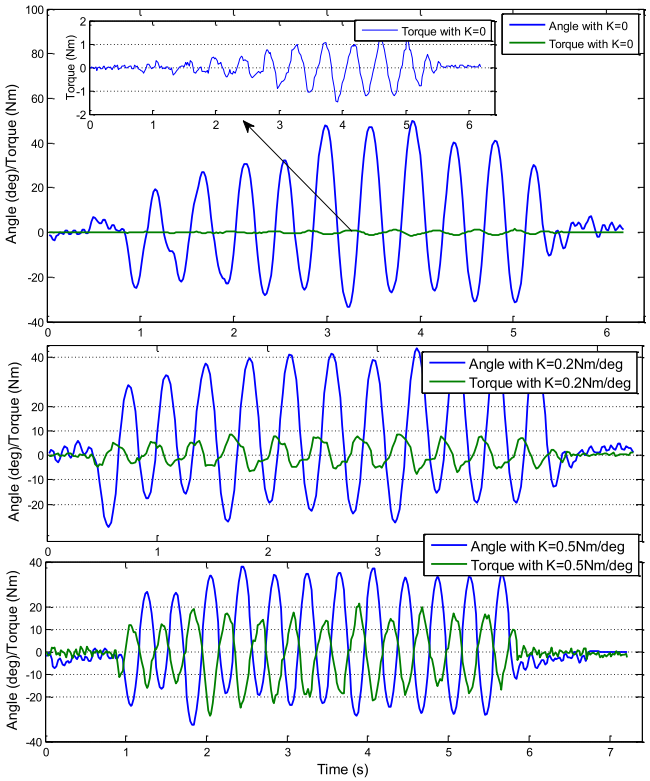

Fig. 8. Validation of the admittance controller for different stiffness.

torque was also near zero, with minor peaks at approximately 0.4 N·m. As the frequency of the excitation increased, the interaction torque continued to oscillate with peak heights below 1.3 N·m. At all frequencies tested, the zero-impedance control was stable. Fig. 8 also shows that for the same angle, different interaction torques (different compliance patterns) can be realized by varying the stiffness ($K = 0.2$ and $K = 0.5$).

B. Evaluation of the Controller

1) Experimental Protocol: All experimental protocols were approved by the Institutional Review Board at the University of North Carolina at Chapel Hill, and three healthy subject (males, age 28 ± 3, weight $78 \pm 5\,\mathrm{kg}$, height $174 \pm 3.0\,\mathrm{cm}$) provided consent before the experiments.

Subjects were asked to perform normal walking on a treadmill at their preferred walking speed. A cable suspension system (Zero-G, Aretech, Washburn, VA, USA) was connected to the subject via straps in the backpack vest to prevent falling.

Three experiments were conducted to evaluate the proposed controller. Experiment I was performed to demonstrate the capacity of the exoskeleton to adjust the weight shaft and step width to improve walking stability. Experiment II aimed to assess the capacity of the controller to assist balance recovery. Experiment III examined whether the exoskeleton could effectively provide the AAN assistive torque to improve balance control. For each experiment, different sets of initial impedance properties were used for different gait phases, and an example is shown in Table II. Damping values were held constant and joint stiffness could be changed by the controller throughout the trials to achieve synergy and compliance as discussed in Section II. Before experiment, every subject was asked to walk at treadmill with self-closed speed to determine the thresholds.

During the experiment I, the subject's equilibrium angles were set to zero during double support, and the subject was asked to walk on a treadmill at a speed of 0.45 m/s. During the experiment II, the HFE's equilibrium angles were set to be nonzero at double support phase, and the gait phases were slightly modified to evaluate the controller's flexibility and generate more natural gait patterns. The subject was asked to walk on a treadmill at a slightly higher speed of 0.65 m/s. During the experiment III, impedance and angle values were set back to the value of the experiment I, and the majority of perturbations were given at the same gait phase (left-leg early swing). Manual pushes were given by an experimenter from one side of the treadmill during single support phase for each leg. Placebo pushes were sporadically introduced to prevent subjects' adaptation and anticipatory responses.

TABLE II
IMPEDANCE PARAMETERS

Gait phase		Stiffness ($\mathrm{N{\cdot}m/deg}$)		Damping($\mathrm{N\cdot m/deg\cdot s^{-1}}$)		Equilibrium angle (°)	
		HFE	HAA	HFE	HAA	HFE	HAA
Set I/III	ES	0.6	0.2	0.06	0.02	40	0
	LS	0.6	0.2	0.06	0.02	0	0
	stance	0.2	0.2	0.02	0.02	−10	0
Set II	ES	0.6	0.2	0.06	0.02	MHFA	CO
	LS	0.6	0.2	0.06	0.02	0	CO
	stance	0.2	0.2	0.02	0.02	MHEA	CO

ES- early swing, LS- later swing, MHFA- maximum hip flexion angle, MHEA- maximum hip extension angle, CO- Controller outputs.

2) Results:

Experiment I: The experimental results from a representative trial are shown in Fig. 9. During normal walking, the weight shift ratios and CoMy varied little within a given period (e.g., a swing phase). The weight shift ratios in the sagittal and frontal planes during this test can be estimated from the test data. The weight shift ratio in the sagittal plane, r_{lateral}, remained within

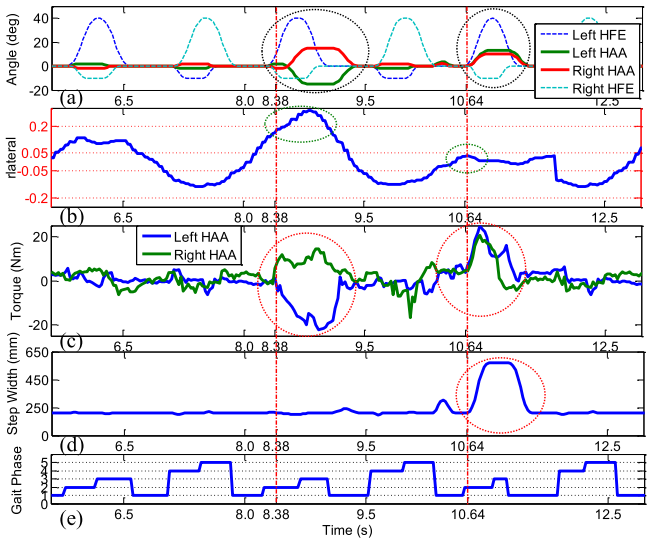

Fig. 9. Results for straight walking with step-width correction. (a) Joint angles. (b) Weight shift ratios in the lateral plane, r_{lateral}. (c) Interact torque. (d) Step width. (e) Gait phase. Gait phases: 1- double support, 2- left-leg early swing (flexion), 3- left-leg late swing (extension), 4- right-leg early swing (flexion), 5- right-leg late swing (extension). The red vertical lines indicate the times of the perturbations.

a range with an upper threshold of 0.2 and a lower threshold of 0.05 during the left-leg swing, whereas r_{lateral} remained within a range between an upper threshold of –0.05 and a lower threshold of –0.2 during the right-leg swing.

In this trial, perturbations were introduced at approximately 8.38 s (the first vertical red dashed line) and 10.64 s (the second vertical red dashed line). After the onset of the first and second perturbations, the weight shift ratio in the frontal plane exceeded the preset maximum and minimum thresholds, respectively.brk For the perturbation applied at 8.38 s, the current gait phase was the left-leg swing, and the perturbation was from the swing side to the stance side. This resulted in both HAA joints attempting to shift the wearer's weight to his left leg to avoid further tilting to the right. For the perturbation applied at 10.64 s, the current gait phase was also the left-leg swing, but the direction of the perturbation was reversed. The results showed higher hip abduction levels in both joints at the heel strike and a wider step width, as seen in Fig. 9(d). After each perturbation, all angle changes returned to their values for normal walking. The measured interaction torques applied by the HAA joints also synchronized with the angle changes to assist in balance recovery throughout the trial. During the period after a perturbation, the torque profile deviated from the values observed during normal walking to accommodate the sudden perturbation. For example, at approximately 8.38 s, both of the hip exoskeleton's HAA joints offered assistive torque to help the subject shift his weight to recover balance. Similarly, at 10.64 s, both HAA joints generated assistive torque to help the subject broaden his step width to retain balance.

Experiment II: The experimental results from a representative trial are shown in Fig. 10. For the subject 2, the weight shift ratio in the sagittal plane, r_{lateral}, remained within a range with an upper threshold of 0.1 and a lower threshold of 0.025 during

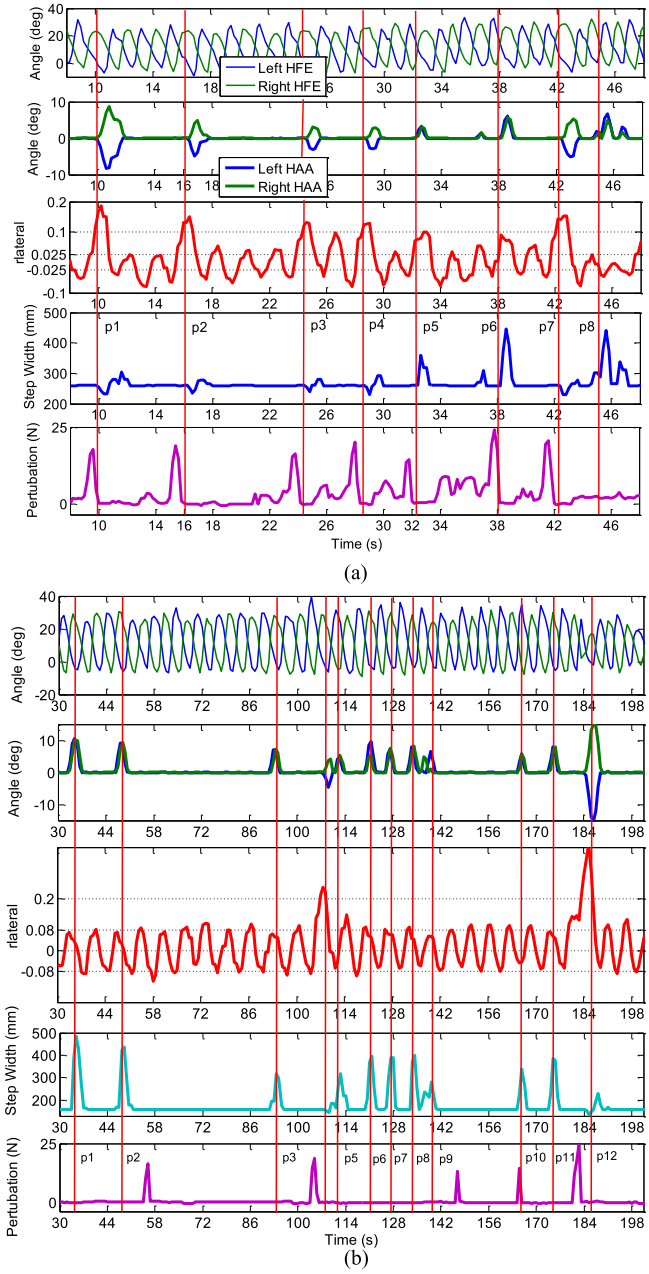

Fig. 10. Results of subject 2 walking with perturbations. The red vertical lines indicate the times of the perturbations. (a) Results of subject 2. (b) Results of subject 3.

the left-leg swing, whereas r_{lateral} remained within a range between an upper threshold of –0.025 and a lower threshold of –0.1 during the right-leg swing. The thresholds of subject 3 are ± 0.08 and ± 0.2. The perturbations were recorded at experiment II.

Table III summarizes the controller performance in controlling the peak HAA angles, peak step width, peak weight shift, as well as the peak amount of deviation of r_{lateral} from the preset thresholds of the each perturbation profiles. For the subject 2, the perturbations 1, 2, 3, 4, and 7 were applied on the swing leg side during the right-leg single support gait phase, the hip exoskeleton assist shift weight to swing leg side to help subject to balance recovery; the perturbations 5 and 6 were applied on

TABLE III
SUMMARIZES THE RESULTS OF EXPERIMENT II

S	#	PD	PA (N)	GP	DT	HAA (L/R°)	SW (mm)	WS (°)
2	p1	PI	17.5	5	0.1	−9/9	300	7.5
	p2	PI	18	5	0.05	4.5/−4.5	300	6
	p3	PI	16.5	5	0.04	−3/3	300	5.6
	p4	PI	20	4	0.04	−3/3	310	6.6
	p5	PIII	15	5	0.01	3/3	350	4
	p6	PIII	24.5	4	0.02	6/6	440	3.6
	p7	PI	20	5	0.06	−6/6	290	7.2
	p8	PII	5	3	0.025	6/7	438	−3.1
3	p1	PII	–	5	0.04	10/10	480	5
	p2	PII	–	5	0.035	9/9	440	4.8
	p3	PII	–	5	002	7/7	300	4.7
	p4	PI	20	5	0.05	−4/4	170	12
	p5	PII	–	3	0.01	5/4	310	−4.6
	p6	PII	–	5	0.02	6/9	405	4.8
	p7	PII	–	5	0.025	7/7	400	4.8
	p8	PII	–	5	0.03	8/8	406	4.9
	P9	PII	–	5	0.02	2/6	290	4.2
	p10	PII	18	2	0.04	6/6	320	−4.4
	p11	PII	–	5	0.03	8/8	380	4.8
	p12	PI	25	4	0.2	−15/15	240	16

S-subject, PD-perturbation direction, PA- perturbation amplitude, P-gait phase, DT- peak deviation from threshold, SW- peak step width, WS- peak weight shift, L-left, R-right, PI-perturbation were applied on the swing leg side during the right-leg single support gait phase (gait phase 2 or 3), PII- perturbation were applied on the support leg side during left-leg single support gait phase (gait phase 4 or 5), PIII- perturbation were applied on the support leg side during right-leg single support gait phase (gait phase 2 or 3).

the support leg side during right-leg single support gait phase and the perturbation 8 was applied on the support leg side during left-leg single support gait phase, the exoskeleton assist to broaden step width to help subject to balance recovery. The result shows that HAA adjustments were correlated with the amount of deviation of r_{lateral} from the preset thresholds. For example, at perturbation 1 (about 10 s), the deviation of r_{lateral} from the preset threshold was about 0.1 with corresponding left and right HAA angles of about –9/9 (deg), while the HAA angles were –6/6 (deg) when the deviation of r_{lateral} from the preset threshold was 0.05 at perturbation 2 (about 16 s). For the subject 3, the perturbations 4 and 12 were applied on the swing leg side during the right-leg single support gait phase, while other perturbations were applied on the support leg side during left-leg single support gait phase. At perturbation 1, the deviation of r_{lateral} from the preset threshold was about 0.04 with corresponding step width of about 480 mm, while the step width was 300 mm when the deviation of r_{lateral} from the preset threshold was 0.02 at perturbation 3. At perturbation 4, the deviation of r_{lateral} from the preset threshold was about 0.05 with corresponding weight shift of about 12°, while the weight shift were 16° when the deviation of r_{lateral} from the preset threshold was 0.05 at perturbation 12. The HAA angles were not zero during the double-support gait phase, which differed from the results in Fig. 10 due to equilibrium angle changes in the finite-state-machine.

Experiment III: Two representative trials for this experiment set are shown in Fig. 11. In both trials, the same perturbations were given from the swing and stance sides at the second and fourth gait cycles, respectively. Although the resulting angles were nearly identical, the HAA interaction torque profiles

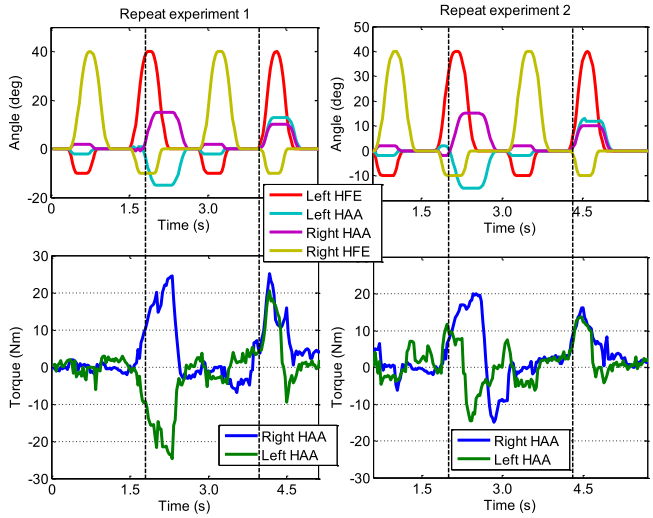

Fig. 11. Left—Experiment III-1. Right—Experiment III-2.

changed to adapt to the mechanical demands of the subject. For the first perturbation, the peak assistance torque for experiment III-1 was 25 N·m while the peak assistance torque for repeat experiment III-2 was 20 N·m. For the second perturbation, the peak assistance torque at experiment III-1 was 25 N·m while the peak assistance torque at experiment III-2 was 16 N·m.

VI. DISCUSSION

The proposed new hip exoskeleton aims to assist individuals with some mobility. HAA and HFE joints on both limbs include powered actuators to actively maintain balance in the sagittal and frontal planes. SEAs are employed in actuation modules, and the powered joints are designed based on admittance control. This allowed the device to achieve passive and software-controlled active compliance when interacting with the wearer. The powered HAA joints are actively controlled using the XCoM concept, assisting with changes in step width and lateral weight shift. Our preliminary results show the promise of our device to improve lateral stability.

The hip exoskeleton can assist a wide range of individuals, such as older adults or those with moderate neurological deficits, who have muscular weakness but retain a certain level of voluntary motor control of their lower limbs. The control in the frontal plane is flexible and can be adjusted based on each subject's unique physical ability. This can be seen in our results for experiments I and II in which the controller provided timely and effective assistance for balance recovery in the frontal plane for different controller sets.

Our device also considered the wearers' efforts to provide appropriate assistance during balance recovery based on an AAN strategy. Fig. 10 demonstrated that subjects' responses to lateral perturbations were not strongly correlated to the magnitude and timing of the perturbations. One explanation for this is that subjects may respond and recover differently to similar perturbations. The proposed hip exoskeleton's assistance depends on the subject's response. For example, the hip exoskeleton will assist more with balance recovery when the subject makes little effort

to recover balance on their own, and assist less when the subject makes a greater effort toward balance recovery. This was validated in experiment III in which HAA assistance torques differed under similar angle profiles after perturbations. The balance recovery strategy continuously monitors the human–exoskeleton interaction in such a way that all four actuators achieve compliance and synergy with wearers. To do this, the applied actuator torque can be modified by varying the joint stiffness parameter, which acts based on the wearers' performance [41]. Due to humans' adaptability and prediction for the perturbation, as well as the wearer's psychological variety, the balance recovery effort of the wearer for the same balance loss condition will be different. Beyond the work of Wang *et al.* [21], [22] in which a fixed, predefined gait trajectory based on the XCoM is enforced; our device provides assist-as-need assistance, which is safer and more effective for wearers who retain partial voluntary control.

Compared with other hip exoskeletons [24]–[31] that are currently used for patients with lower-limb disabilities and older adults, our device offers several structural advantages. First, the weight of the proposed hip exoskeleton is lighter than 10 kg and can supply a continuous torque of 40 N·m for both HFE and HAA. The high-power design along with simultaneous HFE and HAA actuation allows our exoskeleton to be potentially suitable for individuals with more severe physical impairments. Our device's SEA-driven HAA joints can provide additional compliant assistive torque to broaden step width and shift weight to improve lateral stability. Furthermore, our SEAs include joint torque sensors to monitor the interaction torque between exoskeleton and wearer in real time. The controller is applied with human-in-the-loop, which considers the interaction torque between the human and machine to adjust the assistance level.

Our findings indicated that actively assisting with lateral motion could potentially improve gait stability and reduce dependence on external balance aids such as crutches and walkers, if the wearer maintains a certain level of active locomotion control. The controller in the hip exoskeleton does not require the user to wear any additional sensors, which measure electrophysiological activity, such as electromyography electrodes, in quantifying human–robot interaction, is computationally efficient. Given these advantages, the device could be practical for daily-life scenarios, where exoskeletons are expected to provide the most benefit for wearers.

However, our balance recovery assistance method, intended to assist with balance recovery when needed, still has limitations. First, a loss of balance can be induced by a number of perturbation events, such as slipping, tripping, and stumbling. The balance controller presented in this paper is not sensitive to some of these types of perturbations, such as slipping [42]. It will be extremely important to understand the limits of both the detection and balance recovery algorithms under different instability conditions. Second, the human-in-the-loop design still does not fully consider the wearer's effort in balance recovery. Whenever the exoskeleton and human generate input signals to the human–exoskeleton coupled system in a closed-loop manner, a lack of coordination between them can compromise stability. Although the admittance controller will adjust the joint stiffness based on the interaction torque feedback, the interaction torque will instantly increase when the exoskeleton assistance strongly conflicts with the natural way of human balance recovery. The wearer-exoskeleton system must become a "symbiotic" union, with the artificial system predominantly enhancing function while generating little or no disturbance to the wearer [42].

VII. Conclusion and Future Work

This paper describes a novel design and implementation of a hip exoskeleton. The hip exoskeleton includes powered HFE and HAA joints to supporting walking and walking balance. Each actuation unit employs a modular and compact SEA with a high torque-to-weight ratio to make the exoskeleton passively compliant. The online balance controller based on the XCoM concept helps to maintain the gait stability of the coupled human–exoskeleton system. The hip exoskeleton applies assistance as needed by exerting a compliant guidance force on the leg that requires assistance during balance control based on an adaptive admittance control strategy. The results of an experimental verification demonstrate the promising potential of the proposed hip exoskeleton for use as an assistance tool for walking and balance. With the current implementation of the hip exoskeleton prototype and balance control, stable walking without crutches has thus far been achieved only for a healthy subject. Further, research and engineering development is needed to make our device useful for clinical populations or older adults. Moreover, further research will focus on balance control in response to other types of perturbations, using our hip exoskeleton as the test platform.

References

[1] A. M. Dollar and H. Herr, "Lower extremity exoskeletons and active orthoses: Challenges and state of the art," *IEEE Trans. Robot.*, vol. 24, no. 1, pp. 144–158, Feb. 2008,

[2] T. Yana, M. Cempinia, C. M. Oddoa, and N. Vitielloa, "Review of assistive strategies in powered lower-limb orthoses and exoskeletons," *J. Robot. Auton. Syst.*, vol. 64, no. C, pp. 120–136, 2015,

[3] A. J. Young and D. P. Ferris, "State-of-the-art and future directions for lower limb robotic exoskeletons," *IEEE Trans. Neural Syst. Rehabil. Eng.*, vol. 25, no. 2, pp. 171–182, Feb. 2017, doi: 10.1109/TNSRE.2016.2521160.

[4] ARGO Medical Technology, Ltd., 2016. [Online]. Available: http://rewalk.com/rewalk-personal-3/

[5] Ekso Bionics, 2016. [Online]. Available: http://eksobionics.com/

[6] Cyberdyne, 2016. [Online]. Available: https://www.cyberdyne.jp/english/products/HAL/

[7] S. A. Murray, K. H. Ha, C. Hartigan, and M.Goldfarb, "An assistive control approach for a lower-limb exoskeleton to facilitate recovery of walking following stroke," *IEEE Trans. Neural Syst. Rehabil. Eng.*, vol. 23, no. 3, pp. 441–449, May 2015.

[8] C. D. MacKinnon and D. A. Winter, "Control of whole body balance in the frontal plane during human walking," *J. Biomech.*, vol. 26, no. 6, pp. 633–644, 1993.

[9] A. D. Kuo, "Stabilization of lateral motion in passive dynamic walking," *Int. J. Humanoid Robot.*, vol. 18, no. 9, pp. 917–930, 1999.

[10] W. McIlroy and B. Maki, "Do anticipatory postural adjustments precede compensatory stepping reactions evoked by perturbation?," *Neurosci. Lett.*, vol. 164, no. 1, p. 199–202, 1993.

[11] J. Pratt *et al.*, "Capture point: A step toward humanoid push recovery," in *Proc. 2006 6th IEEE-RAS Humanoid Robots*, Genova, Italy, Dec. 2006, pp. 200–207.

[12] A. L. Hof *et al.*, "The condition for dynamic stability," *J. Biomech.*, vol. 38, no. 1, pp. 1–8, 2005.

[13] A. L. Hof, "The 'extrapolated center of mass' concept suggests a simple control of balance in walking," *Hum. Movement Sci.*, vol. 27, no. 1, pp. 112–125, 2008.
[14] A. L. Hof and J. Duysens, "Responses of human hip abductor muscles to lateral balance perturbations during walking," *Exp. Brain Res.*, vol. 230, no. 3, pp. 301–310, 2013.
[15] L. Li, K. H. Hoon, A. Tow, P.H. Lim, and K. H. Low, "Design and control of robotic exoskeleton with balance stabilizer mechanism," in *Proc. 2015 IEEE/RSJ Int. Conf. Intell. Robots Syst.*, Hamburg, Germany, Sep. 2015, pp. 3817–3823.
[16] Evryon exoskeleton, 2016. [Online]. Available: http://www.evryon.eu/index.html
[17] MINDWALKER exoskeleton, 2016. [Online]. Available: https://www.utwente.nl/ctw/bw/research/projects/MINDWALKER/
[18] D. A. Winter, *Biomechanics and Motor Control of Human Movement*. Hoboken, NJ, USA: Wiley, 2009.
[19] B. Ugurlu *et al.*, "Variable ankle stiffness improves balance control: Experiments on a bipedal exoskeleton," *IEEE/ASME Trans. Mechatronics*, vol. 21, no. 1, pp. 79–87, Feb. 2016.
[20] L. Wang, S. Wang, E. H. F. V. Asseldonk, and H. V. D. Kooij, "Actively controlled lateral gait assistance in a lower limb exoskeleton," in *Proc. 2013 IEEE/RSJ Int. Conf. Intell. Robots Syst.*, Tokyo, Japan, Nov. 2013, pp. 965–970.
[21] S. Wang *et al.*, "Design and control of the MINDWALKER exoskeleton," *IEEE Trans. Neural Syst. Rehabil. Eng.*, vol. 23, no. 2, pp. 277–286, Mar. 2015.
[22] D. Martelli *et al.*, "The effects on biomechanics of walking and balance recovery in a novel pelvis exoskeleton during zero-torque control," *Robotica*, vol. 32, no. 8, pp. 1317–1330, 2014.
[23] J. L. Emken, J. E. Bobrow, and D. J. Reinkensmeyer, "Robotic movement training as an optimization problem: Designing a controller that assists only as needed," in *Proc. IEEE Int. Conf. Rehabil. Robot.*, 2005 pp. 307–312.
[24] F. Giovacchini *et al.*, "A light-weight active orthosis for hip movement assistance," *Robot. Auton. Syst.*, vol. 73, pp. 123–134, 2015.
[25] SUITX. 2017. [Online]. Available: http://www.suitx.com/phoenix
[26] B. G. Do Nascimento, C. B. S. Vimieiro, D. A. P. Nagem, and M. Pinotti, "Hip orthosis powered by pneumatic artificial muscle: Voluntary activation in absence of myoelectrical signal," *Artif. Organs*, vol. 32, pp. 317–322, 2008.
[27] C. L. Lewis and D. P. Ferris, "Invariant hip moment pattern while walking with a robotic hip exoskeleton," *J. Biomech.*, vol. 44, pp. 789–793, 2011.
[28] K. Yasuhara, K. Shimada, T. Koyama, T. Ido, K. Kikuchi, and Y. Endo, "Walking assist device with stride management system," *Honda R&D Tech. Rev.*, vol. 21, no. 2, pp. 57–66, 2009.
[29] Q. Wu, X. Wang, F. Du, and X. Zhang, "Design and control of a powered hip exoskeleton for walking assistance," *Int. J. Adv. Robot. Syst.*, vol. 12, no. 3, pp. 1–11, 2015.
[30] A. T. Asbeck, K. Schmidt, and C.J. Walsh, "Soft exosuit for hip assistance," *Robot. Auton. Syst.*, vol. 73, pp. 102–110, 2015.
[31] T. G. Sugar, E. Fernandez, D. Kinney, K. W. Hollander, and S. Redkar, "HeSA, hip exoskeleton for superior assistance," in *Wearable Robotics: Challenges and Trends (Biosystems & Biorobotics*, vol. 16, J. González-Vargas, J. Ibáñez, J. Contreras-Vidal, H. van der Kooij, J. Pons, Eds., Berlin, Germany: Springer, 2017.
[32] G. A. Pratt and M. M. Williamson, "Series elastic actuators," in *Proc. 1995 IEEE/RSJ Conf. Intell. Robots Syst.*, Pittsburgh, PA, USA, 1995, pp. 399–406.
[33] H. Yu, S. Huang, G. Chen, Y. Pan, and Z. Guo, "Human–robot interaction control of rehabilitation robots with series elastic actuators," *IEEE Trans. Robot.*, vol. 31, no. 5, pp. 1089–1100, Oct. 2015.
[34] G. Mathijssen, D. Lefeber, and B. Vanderborght, "Variable recruitment of parallel elastic elements: Series-parallel elastic actuators (SPEA) with dephased mutilated gears," *IEEE/ASME Trans. Mechatronics*, vol. 20, no. 2, pp. 594–602, Apr. 2015.
[35] A. Mazumdar *et al.*, "Parallel elastic elements improve energy efficiency on the STEPPR bipedal walking robot," *IEEE/ASME Trans. Mechatronics*, vol. 22, no. 2, pp. 898–908, Apr. 2017, doi: 10.1109/TMECH.2016.2631170.
[36] U. Keller, H. J. A. V. Hedel, V. Klamroth-Marganska, and R. Riener, "ChARMin: The first actuated exoskeleton robot for pediatric arm rehabilitation," *IEEE/ASME Trans. Mechatronics*, vol. 21, no. 5, pp. 2201–2213, Oct. 2016.
[37] N. Vitiello *et al.*, "Functional design of a powered elbow orthosis toward its clinical employment," *IEEE/ASME Trans. Mechatronics*, vol. 21, no. 4, pp. 1880–1891, Aug. 2016.
[38] S. Crea *et al.*, "A novel shoulder-elbow exoskeleton with series elastic actuators," in *Proc. 2016 6th IEEE Int. Conf. Biomed. Robot. Biomechatronics*, Singapore, 2016, pp. 1248–1253.
[39] N. Kashiri, J. Malzahn, and N. G. Tsagarakis, "On the sensor design of torque controlled actuators: A comparison study of strain gauge and encoder-based principles," *IEEE Robot. Autom. Lett.*, vol. 2, no. 2, pp. 1186–1194, Apr. 2017.
[40] T. Zhang, M. Tran, and H. Huang, "NREL-Exo: A 4-DoFs wearable hip exoskeleton for walking and balance assistance in locomotion," in *Proc. 2017 IEEE/RSJ Int. Conf. Intelligent Robots Syst.*, 2017, pp. 508–513.
[41] M. Bortole *et al.*, "The H2 robotic exoskeleton for gait rehabilitation after stroke: Early findings from a clinical study," *J. NeuroEng. Rehabil.*, vol. 12, no. 54, pp. 1–14, 2015.
[42] V. Monaco *et al.*, "An ecologically-controlled exoskeleton can improve balance recovery after slippage," *Sci. Rep.*, vol. 7, 2017, Art. no. 46721, doi: 10.1038/srep46721.

Ting Zhang (S'09–M'17) received the Ph.D. degree in mechatronics engineering from the Harbin Institute of Technology, Harbin, China, in 2014.

Since 2015, he has been receiving Postdoctoral training with the UNC/NCSU Joint Department of Biomedical Engineering, University of North Carolina at Chapel Hill and North Carolina State University, Raleigh, NC, USA. His current research interests include the multifingered hand for robots and prostheses, exoskeleton robot, sensors, and human–robot interaction.

Minh Tran received the B.S. degree in mechanical engineering from North Carolina State University, Raleigh, NC, USA, in 2017.

His current research interests include the design and control of rehabilitation devices.

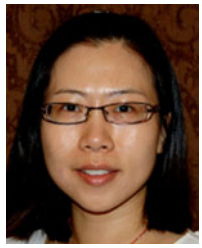

He (Helen) Huang (S'03–M'06–SM'12) received the Ph.D. degree in biomedical engineering from Arizona State University, Tempe, AZ, USA, and the post-doctoral training in neural engineering from the Rehabilitation Institute of Chicago, Northwestern University, Chicago, IL, USA.

She is currently a Professor with the Joint Department of Biomedical Engineering and the Director of the Closed-Loop Engineering for Advanced Rehabilitation (CLEAR) core with North Carolina State University and the University of North Carolina at Chapel Hill, Chapel Hill, NC, USA. Her research interests include neural-machine interfaces for artificial limbs and exoskeletons, human-robot interaction, adaptive and optimal control of wearable robots, and human movement control.